Effect of substrate orientation on lattice relaxation of epitaxial $BiFeO_3$ thin films

Daisuke Kan[a] and Ichiro Takeuchi
Department of Materials Science and Engineering, University of Maryland, College Park, Maryland 20742, USA

(Received 28 January 2010; accepted 15 May 2010; published online 6 July 2010)

We have investigated detailed structural properties of epitaxial $BiFeO_3$ thin films grown on (001), (110), and (111) $SrTiO_3$ substrates in thicknesses up to 1 μm. X-ray reciprocal space mappings reveal that the fabricated films have crystal structures and the strain relaxation dictated by the substrate orientation. The rhombohedral structure, which is observed in the bulk form, is maintained only when the film is grown on the (111)-oriented substrate. The films grown on the (001) and (110)-oriented substrates have a lower structural symmetry than the rhombohedral one, namely a monoclinic structure. Two different processes are observed for the relaxation of the epitaxial strain from the substrate: they are (1) changes in lattice constants and (2) changes in the distortion angle in the $BiFeO_3$ lattice. In the presence of a biaxial strain along the {100} axis, the relaxation in the distortion angle is inhibited, causing a gradual change in the lattice constants. As the number of the {100} axes on the substrate surface is decreased, the distortion angle relaxation becomes the dominant process, making the lattice parameters fully relaxed. We also find that the tilting of the crystallographic domain structures takes place concomitant with the angle relaxation process. These results indicate the strong influence of the substrate orientation on the structural properties of epitaxially-grown $BiFeO_3$ thin films. © *2010 American Institute of Physics*.
[doi:10.1063/1.3452360]

I. INTRODUCTION

Epitaxial thin films suffering from the epitaxial strain due to the lattice mismatch between the material and the substrate often display intriguing phenomena which are not observed in their bulk counterparts. In the case of ferroelectric thin films, for instance, the epitaxial strain can result in enhancement in ferroelectric and dielectric properties[1,2] as well as rotation of the polarization direction[3] because structural deformations and ferroelectricity are closely related to each other.

Bismuth ferrite $BiFeO_3$ (BFO) with a rhombohedral R3c perovskite structure is a material being intensively studied[4] due to its room-temperature multiferroic properties with interesting combinations of magnetic, piezoelectric, and ferroelectric properties.[5,6] In fact, it has been reported that the rhombohedral structure in bulk BFO is modified when the BFO films are epitaxially grown on substrates with different symmetries from the BFO (R3c), e. g., $SrTiO_3$ (STO) which has a cubic symmetry.[7–9] For the epitaxial thin film grown on the (001) STO substrate, the symmetry of the rhombohedral structure becomes lowered to a monoclinic structure with different lattice parameters.[7,8] Moreover, on such a substrate, the polarization direction is rotated up or down with respect to the [111] direction depending on whether the film is under compressive or tensile strain.[3] Recent theoretical studies[10,11] predict strong influence of the substrate-induced strain on the spontaneous polarization of the BFO in the epitaxial thin film form. Given that the strain state varies with changing thicknesses, it is important to understand how the crystal structure evolves as the relaxation of the epitaxial strain with thickness commences.

In this work, we investigate evolution of the structural properties of epitaxally grown BFO on (001), (110), and (111) STO substrates in the thickness range of 50 nm to 1 μm. From x-ray reciprocal space mapping (RSM), we find that the fabricated thin films with thicknesses up to 1 μm have different crystal structures depending on the substrate orientation. The rhombohedral structure is only seen for (111)-oriented films, while the structural symmetry of the (001) and (110) oriented films are lowered from the rhombohedral symmetry to a monoclinic one. The lattice relaxation process also is found to be dependent on the substrate orientation, revealing two dominant strain relaxation processes: relaxation in lattice constants and the distortion angle. Based on the structural evolution, we discuss how the symmetry of the strain from the substrate affects the lattice relaxation processes.

II. EXPERIMENTAL DETAILS

BFO thin films were epitaxially grown on (001), (110), and (111) oriented $SrTiO_3$ (STO) substrates with thicknesses ranging from 50 nm to 1 μm by pulsed laser deposition. Prior to the deposition of the BFO layers, a $SrRuO_3$ (SRO) epitaxial layer was grown as a bottom electrode at the substrate temperature of 700 °C under the oxygen pressure of 100 mTorr. During the deposition of the BFO layer, the temperature and oxygen pressure were maintained at 590 °C and 25 mTorr, respectively. The structural characterizations were performed by RSM with a conventional 4-circle x-ray

[a]Present address: Institute for Chemical Research, Kyoto University, Uji, Kyoto, 611-0011, Japan. Electronic address: dkan@scl.kyoto-u.ac.jp.

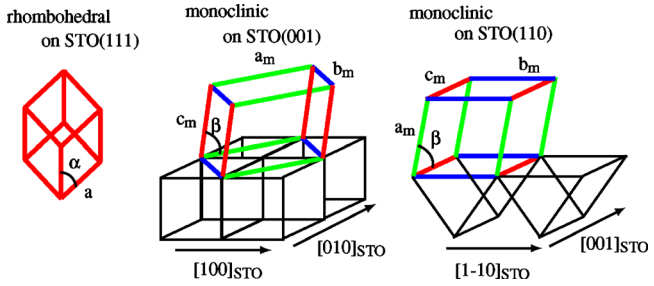

FIG. 1. (Color online) Schematics for crystal structures of epitaxial $BiFeO_3$ thin films grown on (a) (111), (b) (001), and (c) (111) $SrTiO_3$ (STO) substrates. In the figure, the subscript m denotes the monoclinic symmetry.

diffractometer (Bruker D8). The reciprocal lattice unit is normalized by the lattice constant of $SrTiO_3$, 0.3905 nm. No impurity phases were detected with the x-ray diffraction. For electrical characterization, a 100 nm-thick Pd layer was patterned into pads 50×50 μm^2 in size as the top electrodes. The saturated polarization was determined by measuring room-temperature ferroelectric hysteresis loops at 25 kHz with a Radiant Premiere II loop analyzer at room temperature.

III. RESULTS AND DISCUSSIONS

The x-ray RSM reveals that the fabricated thin films have crystal structures which depend on the orientation of the STO substrate. Figure 1 shows schematics of the crystal structures for epitaxial BFO thin films and STO substrates. These structures best capture the experimental observations in this study and are in good agreement with previous reports.[8,9,12] For the (111) oriented film [Fig. 1(a)], the rhombohedral structure is maintained as observed in bulk. The (001) and (110) oriented films have a lowered structural symmetry, namely monoclinic, as drawn in Fig. 1(b) and 1(c), respectively. The epitaxial relationships between the film with the monoclinic structure and the substrate are $[001]_{m,BFO}\|[001]_{STO}$, $[100]_{m,BFO}\|[110]_{STO}$, and $[010]_{m,BFO}\|[1-10]_{STO}$. (The subscript m denotes monoclinic indices.) In these monoclinic structures, the distortion angle in the original rhombohedral structure corresponds to the angle between the $[100]_{m,BFO}$ and $[001]_{m,BFO}$ axes.

Let us start with (111)-oriented BFO thin films. For all the films, there are only (hhh) peaks observed in the 2θ-θ scan. In addition, the ϕ scan of the (010) BFO reflection (not shown) displays three peaks separated by 120° in ϕ, and these three BFO peaks lie at the same ϕ angle as those for the STO substrate. These observations indicate that the fabricated films have a threefold symmetry, which is consistent with the rhombohedral symmetry. Figure 2(a) shows a semilogarithmic contour plot of the RSM around the (312) STO Bragg reflection for the 400 nm-thick film. Only one peak is observed in the RSM, indicating that there is no crystallographic twinning in the film. The observed RSM is consistent with the rhombohedral structure. In Figs. 2(b) and 2(c), we plot the thickness dependence of the lattice constant and the distortion angle α in the cubic notation, respectively. The compressive strain begins to relax below 50 nm. This is in good agreement with previous works[12,13] where the critical thickness for the (111) film was reported to be as thin as 20 nm. With increasing thickness, both the lattice constant and the angle α increase in values, and become constant at 3.966 Å and 89.4° in the thickness region larger than 150 nm. More importantly, the observed angle is almost the same as the one in bulk, while the lattice constant is slightly off the bulk value (3.96 Å) even in the fully-relaxed thick film. This strongly suggests that the angle relaxation is the predominant process for relieving the strain from the substrate. Figure 2(d) shows the saturated polarization value for different thicknesses. The values remain unchanged at ~105 $\mu C/cm^2$, which agrees with the reported values.[14] The constant polarization value with the thickness is consistent with the fact that the structural properties do not depend on the thickness in this range.

Figure 3(a) shows semilogarithmic contour plots of the RSMs around STO (003), (113), and (203) Bragg reflections for the 400 nm-thick (001)-oriented BFO films. The multiple reflections from the BFO layer are observed in the (113) and (203) RSMs, indicating that the multiple crystallographic domain structures have formed. The key observation is that the one reflection with the larger H in the (113) RSM has the same L index as the one for the (003) RSM, while the two reflections in the (203) RSM is slightly shifted up for one and down for the other with respect to the L index of the (003) reflection. This indicates that the film structure has taken the monoclinic structure[8] as depicted in Fig. 1(b). It is worthwhile to note that the ϕ scan of the (011) BFO peak (not shown) clearly has four peaks separated by 90°, which is consistent with the monoclinic structure in Fig. 1(b). Essentially the same features as those for the 400 nm-thick film are

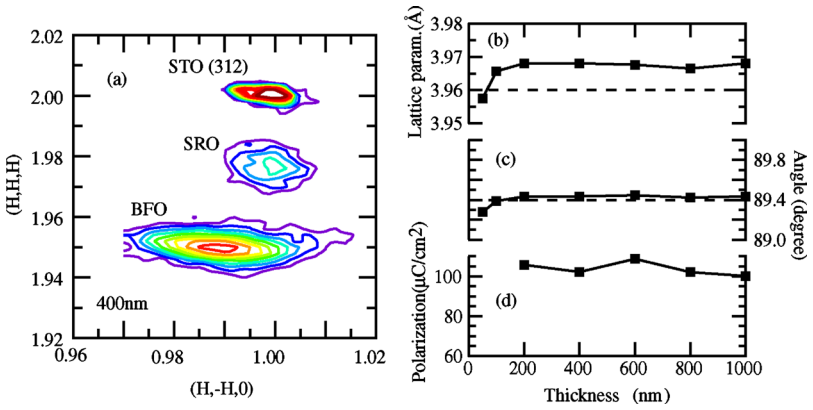

FIG. 2. (Color online) (a) Semilogarithmic contour plot of the x-ray RSM for the 400 nm-thick (111)-oriented $BiFeO_3$ thin film. The mapping was measured around the (312) $SrTiO_3$ Bragg reflection. STO, SRO, and BFO stand for $SrTiO_3$, $SrRuO_3$, and $BiFeO_3$, respectively. (b)–(d) Thickness dependence of the lattice constant (b), angle α (c) and the saturated polarization value (d). The dotted line shows the value for the rhombohedral $BiFeO_3$ in bulk.

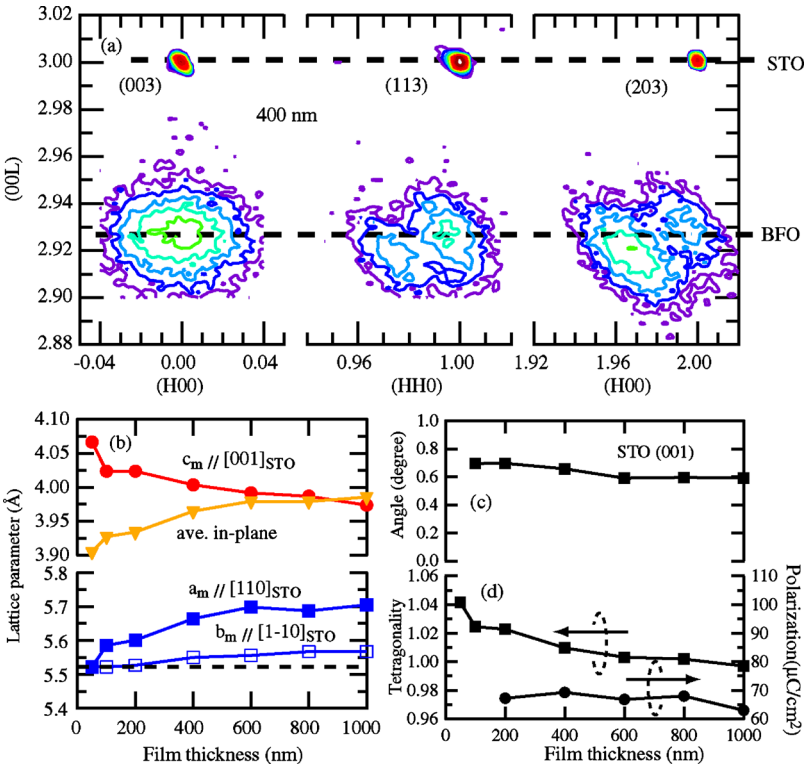

FIG. 3. (Color online) (a) Semilogarithmic contour plots of the x-ray RSM for the 400 nm-thick (001)-oriented $BiFeO_3$ thin film. The mapping was measured around the (003), (113), and (203) $SrTiO_3$ Bragg reflection. (b)–(d) Thickness dependence of the lattice constants (b), angle β (c), and the saturated polarization value (d). In (b), the "average in-plane" is calculated to be $\sqrt{a_m^2+b_m^2}/2$. In (c), the dotted line shows the lattice parameters of the STO substrate. In (d), the tetragonality is defined to be $2c_m/\sqrt{a_m^2+b_m^2}$.

seen for the films in the entire thickness range, indicating that the monoclinic structure is the fully-relaxed structure for this orientation.

The thickness-dependent structural evolution of the (001)-oriented thin films shows a distinct difference from that of the (111)-oriented films. Figures 3(b) and 3(c) show the thickness dependence of the lattice constants and the angle β determined from the RSMs, respectively. Below 50 nm, the in-plane lattice constants are locked-in by the substrate and have the identical value with the STO substrate. The 50 nm-thick film apparently has a tetragonal structure within the resolution of our x-ray diffractometer [the peak splitting in the (113) reciprocal space is not distinguishable.] Beyond the critical thickness of ~50 nm where the lattice relaxation begins to take place, the lattice parameters show a gradual change and, beyond 600 nm, have almost constant values. The distortion angle β also shows the similar trend as seen in Fig. 3(c). The gradual decrease in the value is seen up to 600 nm and beyond this thickness, β has the constant value of ~0.6°. This indicates that the film continues to suffer from the residual strain from the substrate beyond the critical thickness. This is in stark contrast to the structural evolution observed for the (111)-oriented film as seen in Fig. 2(c) and indicates that the lattice relaxation mechanism in (001) films is different. The reason for the gradual change for the (001)-oriented film could be the biaxial strain imposed by the (001) substrate, which could inhibit the relaxation in the angle and results in incomplete strain relaxation at the critical thickness. Figure 3(d) shows the tetragonality defined as $2c_m/\sqrt{a_m^2+b_m^2}$ [see Fig. 1(b)] and values of the saturated polarization at room temperature against the thickness. Due to the lattice deformation associated with the strain relaxation, the tetragonality changes from 1.04 at the thickness of 50 nm to 1.0 at 1 μm. Nonetheless, the observed polarization value remains unchanged at ~65 $\mu C/cm^2$. This observation is in agreement with a previous report.[7] The invariance in the polarization value tells us that the strain relaxation plays little role on the polarization value beyond 200 nm.

Tilting of the (001) plane of the BFO layer is also observed as the thickness is increased. This was revealed by the splitting of the (003) BFO reflection as seen in Fig. 4(a), where the semilogarithmic contour plots of the RSMs for the 1 μm-thick (001)-oriented film taken with the incident x-ray parallel to the [100] and [110] directions are displayed. Two reflections are seen along the [100] (or [010]) direction (ϕ =0°), while along the [110] direction (ϕ=45°) three reflections are observed. These observations correspond to the tilting depicted in Fig. 4(b). This agrees well with the recent report on the rotation of twin structures in 720 nm-thick (001)-oriented BFO thin film.[15] Fig. 4(c) shows the thickness dependence of the tilting angle. Beyond 600 nm, the tilting occurs and the value remains at ~0.3° up to 1 μm. Based on the fact that the lattice constants and the distortion angle β have almost constant values beyond this thickness [Figs. 3(b) and 3(c)], we conclude that the residual strain is relieved through the tilting. Moreover, since the tilting occurs in the plane where β exists, it is not unreasonable to consider that the tilting is associated with the relaxation in the distortion angle which is suppressed in the thinner region.

Figures 5(a) shows the semilogarithmic contour plots of the RSMs for the 400 nm-thick (110)-oriented film. The RSMs were taken around STO (220), (310), and (222) Bragg reflections. The BFO layer exhibits two peaks in each (220) and (222) RSMs. Note that the (220) reflection splits only along the [001] direction and remains a single peak along the $[1\bar{1}0]$ direction. This also agrees with the fact that the single peak is observed in the RSM around the (310) reflection.

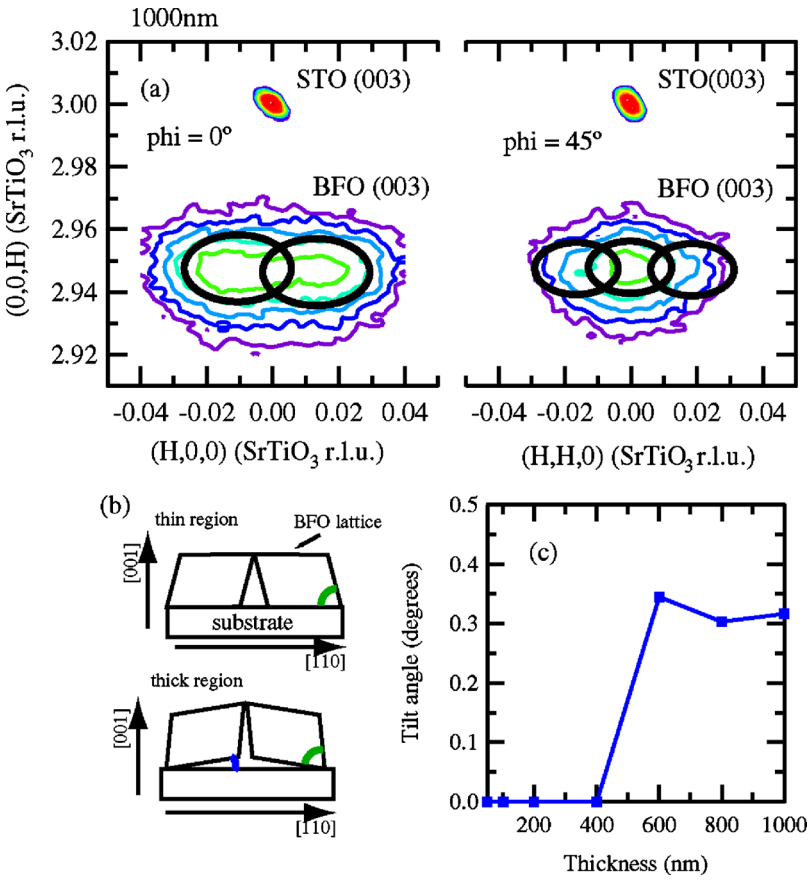

FIG. 4. (Color online) (a) Semilogarithmic contour plots of the x-ray reciprocal space mapping for the 1 μm-thick (001)-oriented $BiFeO_3$ thin film. The mapping was measured around the (003) $SrTiO_3$ Bragg reflection with incident x-ray parallel to the [100] (ϕ =0) and [110] direction (ϕ=45°). For clarity, the thick black ellipses are drawn to indicate the reflections from the $BiFeO_3$ layer. (b) Schematics describing the tilting of the domain structures in the (001) film. (c) Tilt angle [the angle in blue in (b)] plotted as a function of thickness.

Based on the monoclinic cell drawn in Fig. 1(c), the appearance of the two BFO reflections in the (220) RSM can be understood as the existence of two crystallographic domain structures where one of the BFO domain structure is distorted along either the [001] or [00$\bar{1}$] direction and that the (110) plane is tilted up or down with respect to the (110) substrate surface.

The thickness dependence of the lattice parameters and

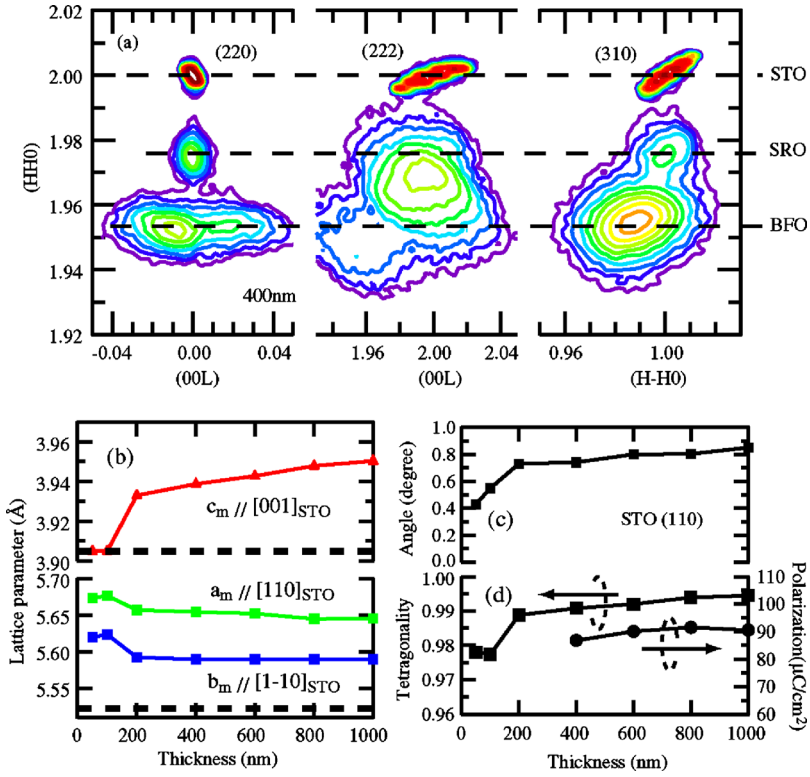

FIG. 5. (Color online) (a) Semilogarithmic contour plots of the x-ray RSM for the 400 nm-thick (110)-oriented $BiFeO_3$ thin film. The mappings were measured around the (220), (222), and (310) $SrTiO_3$ Bragg reflection. (b)–(d) Thickness dependence of the lattice constants (b), angle β (c) and the saturated polarization value (d). In (b), the dotted line shows the lattice parameters of the STO substrate. In (d), the tetragonality is defined to be $2c_m/\sqrt{a_m^2+b_m^2}$.

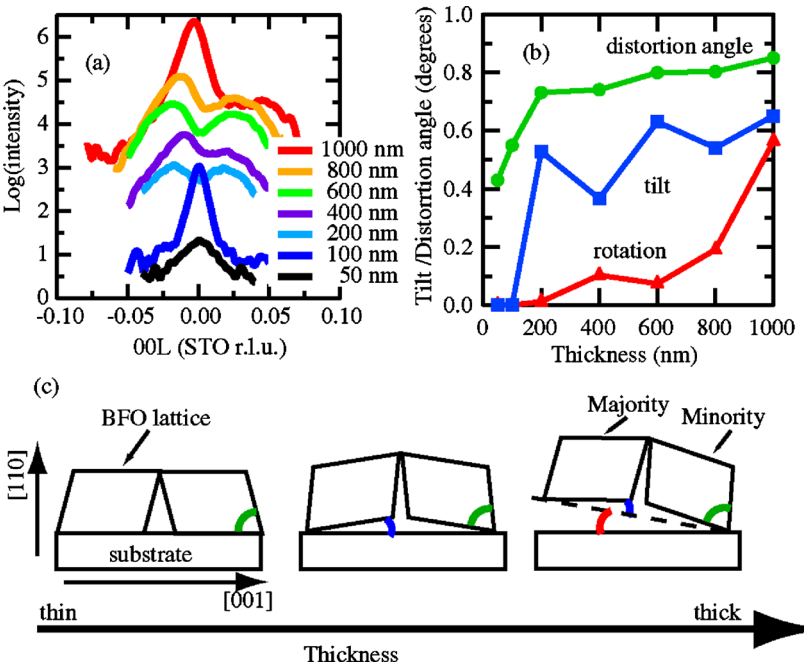

FIG. 6. (Color online) (a) L scans of the (220) $BiFeO_3$ reflection for the (110)-oriented film with thickness up to 1 μm. The scans were performed along the [001] $SrTiO_3$ direction. (b) Evolution of the distortion (green circle), tilting (blue square) and rotation angle (red triangle) for the domain structure in (110) film with thickness. (c) Schematics describing the evolution of the tilting of domain structures in (110) films as a function of thickness.

the distortion angle β determined using the monoclinic cell are plotted in Figs. 5(b) and 5(c), respectively. Due to the anisotropic strain from the (110) substrate, the lattice constants along the [001] (c_m) and [1$\bar{1}$0] (b_m) STO direction show different behaviors. In the thickness less than 100 nm, c_m is locked to the same lattice constant as the substrate, while b_m has the larger value than the one for the substrate. This reveals that the negligible strain along the $[1\bar{1}0]_{STO}$ direction and the contraction in c_m result in the expansion in b_m. As the thickness is increased up to 200 nm, the relaxation takes place exhibiting the distinct change in the lattice constants and β. Beyond this thickness, b_m and β remain constant while c_m shows gradual increase with thickness. This behavior indicates that, for the (110)-oriented film, the stored elastic energy is relieved through the change in not only the lattice constants but also the distortion angle. The uniaxial strain along the [001] direction allows the relaxation in the angle while the biaxial strain for the (001)-oriented BFO thin film keeps the lattice constant fixed, suppressing the angle relaxation process which is only seen in the larger thickness region. Combining our experimental results in Figs. 2, 3, and 5, we can conclude that compressive strain from substrate is mainly applied along the {100} axis and that the distortion angle is predominantly relaxed in the orientation where the compressive strain along the {100} axis is not involved. This is also confirmed by the fact that the thickness where the lattice constants begin to be fully relaxed become smaller as the number of the {100} axes on the substrate surface is decreased.

In Fig. 5(d), the tetragonality ($2c_m/\sqrt{a_m^2+b_m^2}$) and the saturated polarization value at room temperature are plotted against the thickness. Due to the uniaxial strain, the tetragonality becomes lower than 1, from which the slight decrease in the polarization is expected. The observed polarization, however, is 90 $\mu C/cm^2$ which is consistent with the value estimated with the projection rule, $105/(\sqrt{3}/\sqrt{2})$ $\mu C/cm^2$. This indicates again that strain relaxation has little impact on the polarization value beyond 400 nm.

Another interesting behavior is the tilting of the (110) plane associated with the lattice relaxation. Figure 6(a) shows a L scan at the (220) BFO peak along the [001] direction. When the lattice relaxation takes place in the film, the peak begins to split into two peaks (200 nm-thick sample), indicating that the relaxation induces the tilting of the (110) plane of the surface. Note that this tilting is essentially the same as the one observed for the (001) film, revealing that the tilting in connection with the strain relaxation is an intrinsic characteristic of the epitaxially-stabilized monoclinic phase in BFO. The key observation for the (110) film is that the tilt angle varies with thickness and that one of the tilted surfaces of the two domain structures becomes parallel to the substrate surface. The domain structure with the surface parallel to the substrate eventually becomes the dominant one with increasing thickness. This behavior is summarized in Figs. 6(b) and 6(c). When the lattice relaxation occurs, the domains tilt in opposite directions with the angle in blue as shown in Fig. 6(c). Judging from the intensity of the BFO (220) x-ray reflections [Fig. 6(a)], the population of the domain structures tilted in the opposite directions are equally distributed. As the thickness is increased further, both of the domains are rotated in the same direction [the angle in red in the Figs. 6(b) and 6(c)]. This results in one of the (110) surfaces of the domain structures becoming parallel to the substrate surface. It should be noted that the domain with the surface parallel to the substrate surface shows the prominent x-ray diffraction peak, indicating that this is the major domain. The population of the other domain structure decreases with increasing thickness. This observation implies that the {100} twin boundary where the domain with the distortion in

opposite directions (along the [001] and [00$\bar{1}$] directions) faces each other is energetically unfavorable in the BFO lattice (Fig. 6).

Finally, it is interesting to compare the tilting behavior between the (001) and (110) films. Although the tilting itself is essentially the same for two films, the tilting angle in the (110) film is almost double the angle in the (001) film. In addition, the thickness at which the tilting occurs is smaller for the (110) film as compared to the (001) film. These are all consistent with the fact that there is no constrain on the angle relaxation in the (110) film while the biaxial strain in the (001) film suppresses the angle relaxation. This demonstrates the impact of the substrate orientation on not only the crystal structure (and the structural symmetry) in the thin film but also the strain relaxation processes.

IV. SUMMARY

In summary, we have investigated the detailed structural properties of the epitaxial BFO thin films grown on (001), (110), and (111)-oriented STO substrates with thickness up to 1 μm. We found that the orientation of the substrates has a strong influence on not only the structural symmetry but also the strain relaxation process. The rhombohedral structure, as observed for the bulk BFO, is maintained only on the (111) oriented substrate. The films grown on (001) and (110) substrates have a monoclinic structure. We also found that there are two strain relaxation processes in BFO thin films, namely, the relaxation in the distortion angle and relaxation in the lattice constants. The dominant process depends on the substrate orientation which in turn determines the symmetry and the directions of the strain. The biaxial strain imposed by the (001) substrate suppresses the angle relaxation process, causing the gradual change in the lattice parameters. The angle relaxation process was found to become the dominant process as the number of the {100} axes on the substrate surface is decreased. In the epitaxially-stabilized monoclinic phase, the angle relaxation process induces the tilting of the crystallographic domain structures. The observed orientation dependence in the structural evolution is seen even in thickness regions beyond the critical thickness, revealing the strong influence of the substrate orientation on the structural characteristics of the BFO epitaxial thin films.

ACKNOWLEDGMENTS

This work was supported by UMD-NSF-MRSEC (Grant No. DMR 0520471), and ARO (Grant No. W911NF-07-1-0410). The work was also supported by the W. M. Keck Foundation and NEDO.

[1] J. H. Haeni, P. Irvin, W. Chang, R. Uecker, P. Reiche, Y. L. Li, S. Choudhury, W. Tian, M. E. Hawley, B. Craigo, A. K. Tagantsev, X. Q. Pan, S. K. Streiffer, L. Q. Chen, S. W. Kirchoefer, J. Levy, and D. G. Schlom, Nature (London) **430**, 758 (2004).
[2] K. J. Choi, M. Biegalski, Y. L. Li, A. Sharan, J. Schubert, R. Uecker, P. Reiche, Y. B. Chen, X. Q. Pan, V. Gopalan, L.-Q. Chen, D. G. Schlom, and C. B. Eom, Science **306**, 1005 (2004).
[3] H. W. Jang, S. H. Baek, D. Ortiz, C. M. Folkman, R. R. Das, Y. H. Chu, P. Shafer, J. X. Zhang, S. Choudhury, V. Vaithyanathan, Y. B. Chen, D. A. Felker, M. D. Biegalski, M. S. Rzchowski, X. Q. Pan, D. G. Schlom, L. Q. Chen, R. Ramesh, and C. B. Eom, Phys. Rev. Lett. **101**, 107602 (2008).
[4] G. Catalan and J. F. Scott, Adv. Mater. **21**, 2463 (2009).
[5] J. Wang, J. B. Neaton, H. Zheng, V. Nagarajan, S. B. Ogale, B. Liu, D. Viehland, V. Vaithyanathan, D. G. Schlom, U. V. Waghmare, N. A. Spaldin, K. M. Rabe, M. Wuttig, and R. Ramesh, Science **299**, 1719 (2003).
[6] T. Zhao, A. Scholl, F. Zavaliche, K. Lee, M. Barry, A. Doran, M. P. Cruz, Y. H. Chu, C. Ederer, N. A. Spaldin, R. R. Das, D. M. Kim, S. H. Baek, C. B. Eom, and R. Ramesh, Nature Mater. **5**, 823 (2006).
[7] D. H. Kim, H. N. Lee, M. D. Biegalski, and H. M. Christen, Appl. Phys. Lett. **92**, 012911 (2008).
[8] G. Xu, H. Hiraka, G. Shirane, J. Li, J. Wang, and D. Viehland, Appl. Phys. Lett. **86**, 182905 (2005).
[9] G. Xu, J. Li, and D. Viehland, Appl. Phys. Lett. **89**, 222901 (2006).
[10] J. X. Zhang, Y. L. Li, Y. Wang, Z. K. Liu, L. Q. Chen, Y. H. Chu, F. Zavaliche, and R. Ramesh, J. Appl. Phys. **101**, 114105 (2007).
[11] J. X. Zhang, D. G. Schlom, L. Q. Chen, and C. B. Eom, Appl. Phys. Lett. **95**, 122904 (2009).
[12] H. Béa, M. Bibes, X.-H. Zhu, S. Fusil, K. Bouzehouane, S. Petit, J. Kreisel, and A. Barthelemy, Appl. Phys. Lett. **93**, 072901 (2008).
[13] S. Ryu, J.-Y. Kim, Y.-H. Shin, B.-G. Park, J. Y. Son, and H. M. Jang, Chem. Mater. **21**, 5050 (2009).
[14] J. Li, J. Wang, M. Wuttig, R. Ramesh, N. Wang, B. Ruette, A. P. Pyatakov, A. K. Zvezdin, and D. Viehland, Appl. Phys. Lett. **84**, 5261 (2004).
[15] H. Liu, P. Yang, K. Yao, and J. Wang, Appl. Phys. Lett. **96**, 012901 (2010).